THE JOURNAL OF PHYSICAL CHEMISTRY B

Article

Cite This: J. Phys. Chem. B 2019, 123, 8419−8424

pubs.acs.org/JPCB

Arresting an Unusual Amide Tautomer Using Divalent Cations

Somnath M. Kashid,[†,‡] Reman K. Singh,[§] Hyejin Kwon,[#] Yung Sam Kim,*[,#] Arnab Mukherjee,*[,§] and Sayan Bagchi*[,†,‡]

[†]Physical and Materials Chemistry Division, CSIR-National Chemical Laboratory, Pune 411008, India

[‡]Academy of Scientific and Innovative Research (AcSIR), Ghaziabad-201002, India

[§]Department of Chemistry, Indian Institute of Science Education and Research, Pune 411008, India

[#]Department of Chemistry, Ulsan National Institute of Science and Technology (UNIST), 50 UNIST-gil, Ulsan 44919, Korea

Supporting Information

ABSTRACT: Ion-specific effects on peptides and proteins are key to biomolecular structure and stability. The subtle roles of the cations are far less understood, compared to the pronounced effects of the anions on proteins. Most importantly, divalent cations such as Ca^{2+} and Mg^{2+} are crucial to several biological functions. Herein, we demonstrate that an amide−iminolate equilibrium is triggered by the binding of the divalent cations to the amide oxygen in aqueous solution. The excellent agreement between the experimental and theoretical results confirms the arrest of an unusual amide tautomer by the divalent cations, which is a rarely known phenomenon that might open up an array of applications in chemistry and biology.

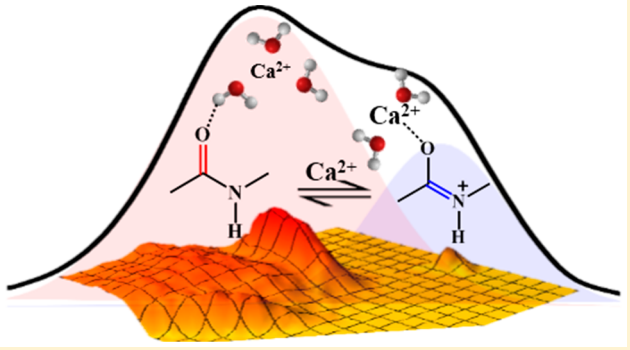

INTRODUCTION

The biological organization is controlled by a delicate balance between noncovalent interactions, in particular those between ions and biomolecules. Ions interact with peptides and proteins through electrostatic forces and have a strong impact on biomolecular structure and stability. The strengths of these protein−ion interactions are regulated by the hydration capacity of the ions. Hofmeister summarized these ion-specific effects according to the capacity of cations and anions to "salt in" and "salt out" the proteins.[1,2] Proposed models to understand the origin of the Hofmeister effect are mainly based on either direct protein−ion interactions or an indirect effect of the ions on the water molecules that solvate the proteins.[3,4] In the indirect interaction model, the ions that enhance the water structure by strengthening the hydrogen-bond network can effectively steal water from the protein and show the salting-out effect. On the other hand, the ions that break the water structure show the salting-in effect. However, recent studies have reported a negligible effect of ions beyond their immediate solvation shells.[5−8] Moreover, pH-dependent studies suggest that the effect of ions on the water hydrogen-bond structure is not sufficient to understand the ordering of the Hofmeister series and the direct protein−ion interactions are important toward protein stabilization.[9,10]

In the recent decade, several experimental and computational studies have been performed using model amides to obtain a deeper insight into ion-specific effects on proteins and peptides.[3,11−14] These studies reveal that the weakly hydrated anions (e.g., NO_3^-, SCN^-) and the strongly hydrated cations (e.g., Ca^{2+}, Mg^{2+}) have favorable interactions with the protein/peptide backbone. The interactions of the cations with the backbone, although less pronounced compared to that of the anions, are far less understood. Among cations, divalent cations such as Ca^{2+} and Mg^{2+} are the most commonly used ions in a multitude of biological functions.[15,16] An earlier study reported that these strongly hydrated divalent cations bind to the oxygen (O) atom of the amide carbonyl (C═O) at a moderate concentration, albeit through a weak interaction.[11] On the other hand, another report proposed an indirect, water-mediated interaction model between a divalent cation and the peptide moiety.[12] Despite the immense importance of the divalent cations in biology, a general consensus on the structural aspect of the peptide backbone upon binding of the divalent cations is missing to date.

In this report, we employed *N*-methylacetamide (NMA), one of the simplest molecules containing the peptide bond, as a suitable proxy to model interactions at the protein backbone. Using a combination of infrared (IR) absorption spectroscopy, and molecular dynamics (MD) simulations followed by quantum calculations, we show that an amide−iminolate tautomerism is triggered by the direct binding of the divalent cations to the amide carbonyl (C═O) group. This finding was further validated by additional experiments and two-dimensional (2D) IR spectroscopy. This intriguing, yet unusual

Received: September 5, 2019
Revised: September 18, 2019
Published: September 18, 2019

DOI: 10.1021/acs.jpcb.9b08463
J. Phys. Chem. B 2019, 123, 8419−8424

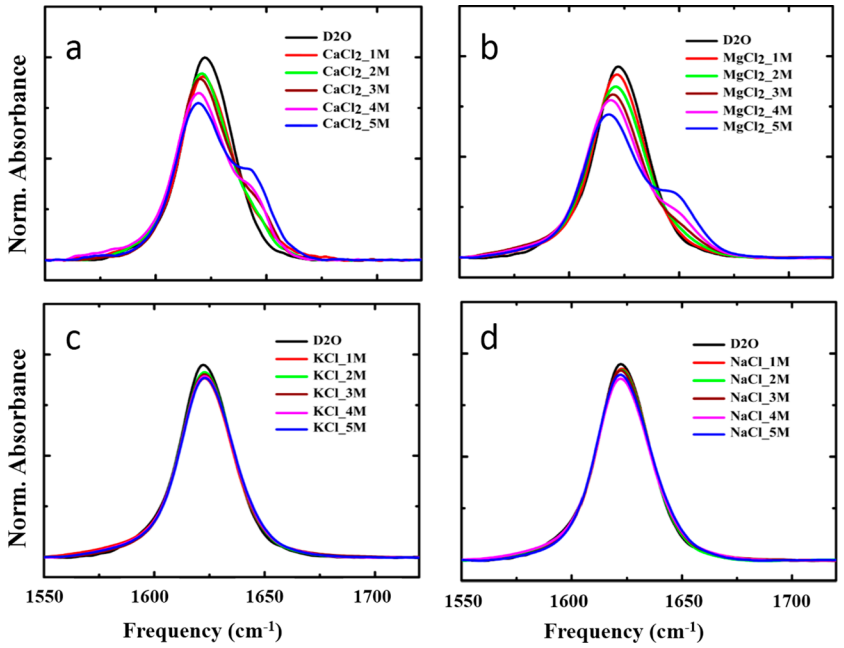

Figure 1. IR spectra of NMA with different (a) $CaCl_2$, (b) $MgCl_2$, (c) KCl, and (d) NaCl concentrations. The spectrum without ion is also shown for reference. All the spectra have been normalized to the area under the curve.

phenomenon, was only observed for divalent cations and might open up an array of applications in chemistry and biology.

METHODS

IR Absorption Experiments. The carbonyl compounds such as acetone, ethyl acetate (EtOAc), *N*-methylacetamide (NMA), *N*,*N*-dimethylacetamide (DMA), urea, and *p*-nitro acetanilide, were obtained from Sigma–Aldrich and used without further purification. Aqueous salt solutions of $CaCl_2$, $MgCl_2$, KCl, and NaCl were prepared with five different concentrations (such as 1, 2, 3, 4, and 5 M) for each set of experiments. All carbonyl compounds were separately dissolved in different aqueous salt solutions and in pure water (D_2O) to prepare the final concentration of 40 mM for IR study. We have also performed IR experiments in aqueous HCl solution to study direct protonation. The Fourier transform infrared (FTIR) absorption spectra were recorded on a Bruker V70 FTIR spectrometer with 1 cm^{-1} resolution at room temperature. For each sample, a sample solution of ∼60 μL was loaded into a demountable cell consisting of two windows (CaF_2, 3 mm thickness, Shenzen Laser Co., Ltd.), separated by a Mylar spacer 56 μm thick.

Two-Dimensional Infrared (2D IR) Experiments. The details related to the experimental setup and analysis of 2D IR data have been previously reported.[17,18] The three successive IR pulses with wave vectors $\boldsymbol{k}_1$, $\boldsymbol{k}_2$, and $\boldsymbol{k}_3$, having controlled polarization and tuned to the amide C═O stretching frequency, were applied to the sample to induce the subsequent emission of the vibrational echo. The vibrational echo in the phase-matching direction ($\boldsymbol{k}_s = -\boldsymbol{k}_1 + \boldsymbol{k}_2 + \boldsymbol{k}_3$) is detected by heterodyning it with a local oscillator (LO) pulse, which preceded the echo signal by an interval of ∼1 ps. The signal and LO are combined at the focal plane of a monochromator (Model TRIAX-190) and detected by a 64-element MCT IR array detector (IR Associates). The focal length of the monochromator is 190 mm and the groove density of the grating used in the experiment is 150 lines/mm. All 2D IR spectra shown here, collected at room temperature, represent the real part of the absorptive spectra. The 2D spectra are displayed as the double Fourier transforms of the (τ, t) data set with frequency arguments (ω_τ, ω_t).

Simulation Method. *N*-methylacetamide (NMA) was optimized quantum mechanically using HF/6-31G* basis set in GAUSSIAN03 software.[19] Furthermore, restricted electrostatic potential (RESP) charges[20] on the atoms of NMA were calculated using ANTECHAMBER module of AmberTools software.[21] The general amber force field (GAFF) for NMA was constructed using AmberTools software.[21] The topology and coordinates generated from AmberTools were converted into GROMACS format using a perl program amb2gmx.pl.[22] We have used the same protocol to create the methyl acetate (MeOAc) force field and coordinates. A classical Drude oscillator-based force field[23] for ions, in conjunction with a polarizable model of water (SWM4-DP),[24] was shown to reproduce a large set of thermodynamical parameters against experiment.[23] Therefore, we used the above combination of force fields for ions and water. This combination was shown to provide the correct concentration dependence (up to 7 M) of dielectric permittivity, structure, and dynamics of aqueous NaCl solution, which was not found in a nonpolarizable model of water.[25]

System Preparation. We have prepared four systems: (i) NMA in 5 M of $CaCl_2$ solution, (ii) NMA in 1 M of $CaCl_2$ solution, (iii) MeOAc in 5 M of $CaCl_2$ solution, and (iv) NMA in 5 M of NaCl solution. To create the NMA in 5 M $CaCl_2$ system, we have taken 536 water molecules and 46 $CaCl_2$ molecules in a cubic box with a length of 30 Å. To create the NMA in 1 M system, 536 water molecules and 9 ions (NaCl or $CaCl_2$) were taken. With the same procedure, we have created the MeOAc in 5 M $CaCl_2$ solution system.

For all the four systems, we first performed energy minimization using the steepest descent method,[26] followed by heating to 300 K for 100 ps by using a Berendsen thermostat[27] with a coupling constant of 0.4 ps. During the

DOI: 10.1021/acs.jpcb.9b08463
J. Phys. Chem. B 2019, 123, 8419−8424

heating, we restrained the heavy atoms of NMA/MeOAc molecule with 25 kcal/mol/Å^2. The harmonic restraint was gradually reduced to 0.25 kcal/mol in six steps. In each step, 100 ps equilibration was performed at constant temperature (300 K) and pressure (1 bar) using a Berendsen thermostat and barostat,[27] each with a coupling constant of 0.2 ps, which was then followed by energy minimization using the steepest descent method.[26] All bonds were constrained using LINCS algorithm.[28] The Particle Mesh Ewald (PME) method[29] was used for the electrostatics with a 10 Å cutoff for the long-range interaction. The cutoff for the van der Waals (vdW) interaction was kept at 10 Å. Simulations were performed with a 2 fs time step. At the final equilibration step, we performed the 10 ns unrestrained equilibration by using the Berendsen thermostat and barostat,[27] each with a coupling constant of 0.2 ps. After equilibration, we have performed 110 ns long production run in an NVT ensemble. All the analyses have been performed on the 110 ns long trajectory. All the simulations were performed using GROMACS-4.5.5 version.[30]

DFT Method for IR Frequency Calculation. To investigate the role of Ca^{2+} in the IR spectra of NMA/MeOAc, we performed DFT calculation on the most probable conformations. To choose the most probable conformations, we have selected the frames around the each minima (MIN1, MIN2, and MIN3) and performed cluster analysis based on the Ca^{2+} distances to the molecule and picked up the more populated structure. Thereafter, we performed quantum mechanical ground-state optimization and frequency calculation using density functional theory (DFT) with B3LYP functional and DZV2P basis set, previously used in ab initio calculation.[31]

RESULTS AND DISCUSSION

Linear Absorption Spectroscopy. IR spectroscopy of the amide vibration is a powerful technique to probe the conformations of biomolecules in solution. A single IR peak in the frequency range of 1600−1700 cm^{-1}, arising from the amide-I band, has been reported for NMA in aqueous (D_2O) solution.[32] The amide-I band arises almost exclusively from the C═O stretch, with a small contribution from the NH bend and the C−N stretch. In the presence of divalent cations such as Ca^{2+} and Mg^{2+}, an additional high-frequency shoulder is observed in the IR absorption spectra (see Figures 1a and 1b). The spectra, when fitted to two Gaussian profiles, identifies an additional peak other than the amide-I band in water, blue-shifted by 25 cm^{-1} (22 cm^{-1}) in the presence of Ca^{2+} (Mg^{2+}) ions. The details of the fits are shown in Figure S1 and Table S1 in the Supporting Information. An increase in the concentration of the divalent cations increases the population of the blue-shifted peak. This blue-shifted spectral signature has been previously described to arise from the direct binding of the divalent cations to the amide O,[11] by displacing all water molecules in the vicinity.[14] However, the C═O chromophore being sensitive to the larger electrostatic field exerted by the divalent cations, as compared to water, is expected to show a red-shift, with respect to that found in neat water. Instead, the presence of an additional blue-shifted peak is incongruent and therefore intriguing, more so because this additional peak is not observed in similar experiments using monovalent cations (see Figures 1c and 1d).

Control experiments on other C═O containing molecules without a conjugating nitrogen (N) atom, i.e., ketones (Figure S2 in the Supporting Information) and esters (Figure S3 in the Supporting Information) validate that the blue-shifted population is exclusively for the amides. The ester (ethyl acetate) exhibits an opposite trend, where a blue-shifted shoulder in neat water shows a decrease in population with an increase in salt concentration. It has been previously reported that the blue-shifted shoulder in ethyl acetate arises from different extents of hydrogen bonding of the ester C═O.[17,18] Moreover, unlike NMA in the presence of divalent cations, earlier reports demonstrated that the frequency shift in esters can be explained from the perspective of the exerted electrostatic field.[33] Thus, the opposite trend seen in esters can be explained from the change of C═O hydrogen bonding in the presence of divalent cations. The increase in the blue-shifted population with increasing divalent ion concentration is only observed for amides. This suggests a greater role of the N lone pair in conjugation with the amide C═O in biomolecules than previously perceived upon binding of divalent cations.[11,12,14] To investigate this further, IR absorption experiments were performed on model amides with increased or decreased electron density on the amide N (see Figures S4−S6 in the Supporting Information). In *N*,*N*-dimethylacetamide (DMA), with an increased electron density on N, because of the presence of an extra methyl group, we observe a larger population of the blue-shifted peak (Figure S4 in the Supporting Information). In urea, where two amine groups are in conjugation with the C═O group, an amplification of the blue-shifted population is observed (Figure S5 in the Supporting Information). In contrast, the blue-shifted peak is not observed when an electron-withdrawing (*p*-nitrophenyl) group is attached to the N atom (Figure S6 in the Supporting Information). A probable explanation of these findings is that the lone pair of N possibly stabilizes the negative charge density on the O atom, which, in turn, helps to form the previously described amide−divalent cation contact pair.[14] However, this explanation is in contradiction with a blue-shifted C═O peak.

Molecular Dynamics Simulations. To obtain the molecular understanding of the phenomenon, we resorted to MD simulation (see the Supporting Information for simulation details). We constructed a system of NMA in 5 M Ca^{2+} concentration and ran a 110 ns simulation to obtain the volume-corrected distance distribution of cations, with respect to the amide O and N (Figure 2a), which shows three maxima—MIN1, MIN2, and MIN3 (correspond to minima in free energy). In MIN1, Ca^{2+} interacts directly with the amide O (distance is 2.3 Å) and is located 4.3 Å from the amide N (Figure S7a in the Supporting Information). In MIN2, the most stable state under this condition, Ca^{2+} is 4.5 and 6.3 Å away from the amide O and N, respectively, and makes water-mediated interaction with the O atom (Figure S7b in the Supporting Information). In MIN3, Ca^{2+} is farther away (6.5 Å) from both the amide O and N (Figure S7c in the Supporting Information). However, NMA at the lower Ca^{2+} concentration (1 M) (Figure 2b) does not show the contact minimum (MIN1). Therefore, the contact minimum obtained in the computational result at moderate concentrations of the divalent cations corroborates with the experimental observations of the blue-shifted population under the same conditions. Furthermore, control simulations either on an ester with 5 M Ca^{2+} (Figure S8a in the Supporting Information) or on NMA with 5 M Na^+ (Figure S8b in the Supporting Information) confirmed the absence of the contact minima in such scenarios. Distribution of chloride ions is uniform in all the systems (see

DOI: 10.1021/acs.jpcb.9b08463
J. Phys. Chem. B 2019, 123, 8419−8424

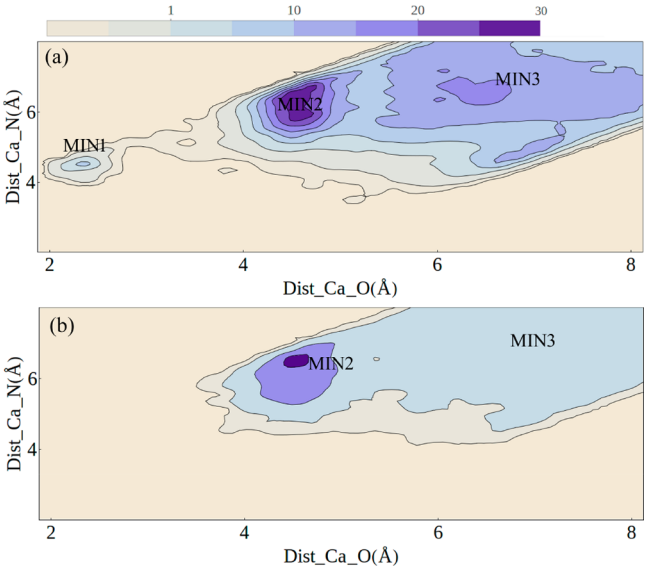

Figure 2. Volume-corrected distance distribution of cations Ca^{2+} around amide O and N atoms of NMA in (a) 5 M $CaCl_2$ and (b) 1 M $CaCl_2$ solution. The maximum of each distribution corresponds to the free-energy minimum, as represented by MIN1, MIN2, and MIN3.

Figures S9a–S9d in the Supporting Information), indicating a rather passive role played by the anion.

A recent ab initio umbrella sampling simulation on NMA predicted the contact geometry between C═O and Ca^{2+}, in terms of free energy, to be the most stable configuration.[14] However, this would contradict the experimental result where the blue-shifted peak appears as a shoulder to the original amide-I band upon the addition of Ca^{2+} ion (Figure 1a). The discrepancy could originate from either overestimation of the interaction between C═O and Ca^{2+} in the ab initio treatment or statistical sampling error associated with a shorter ab initio study.

Quantum Chemical Calculations. To investigate the reason for the above corroboration, we looked into the electronic characteristics of these minima, in terms of their vibrational spectra using density functional theory (DFT) on the most representative structure of the particular minimum (see the Supporting Information for details). Figure 3a shows the vibrational spectra of C═O and C−N stretching frequencies of the amide moiety for all three minima. When Ca^{2+} is away from O (MIN3), C−N stretch appears to be red-shifted, compared to the C═O stretch. As the cation gets closer to O (MIN2 and MIN1), the stronger electrostatic field of Ca^{2+} causes a red-shift to the C═O frequency and, interestingly, a concomitant blue-shift to the C−N frequency. The frequency shift in the opposite direction is large enough in MIN1, where Ca^{2+} is in direct contact with O, to result in a crossover of the C═O and C−N frequencies. Moreover, our calculations predict that the C−N stretch has a high molar extinction coefficient (ε), compared to the C═O stretch (black curve in Figure 3a). Coincidentally, the C−N peak at MIN1 appears at a blue-shifted frequency adjacent to the original amide-I peak, thus giving a false impression that C═O has blue-shifted, as presumed in earlier reports.[11,12] The peak frequencies are given in Table S2 in the Supporting Information.

As MIN2 is more stable than MIN1, the experimental infrared spectra will be a weighted average of the spectra shown in Figure 3a with the weights associated with the stability of the minima. Therefore, the C−N stretch is observed as a blue-shifted shoulder of the original amide-I band in the ensemble-averaged experimental spectrum. No frequency crossover was observed in similar frequency calculations on either a nonamide control system (Figure S10a in the Supporting Information) with 5 M Ca^{2+} or on NMA with 5 M Na^{+} (Figure S10b in the Supporting Information). Thus, computations suggest that the additional peak originates from the C−N stretch of the amide moiety, and not from the C═O stretch. Quite naturally, the subsequent question is why the blue-shift is observed in the C−N stretch at moderate divalent ion concentrations. To obtain an explanation, we performed natural bond orbital (NBO) analysis of NMA in 5 M Ca^{2+}. We found that the bond order of C═O, at MIN1 (Figure 3b), changed from double to single, whereas that of C−N changed from single to double (see Figure S11 and Table S3 in the Supporting Information). At the other minima (MIN2 and MIN3), C═O retains its partial double-bond character, as evident from the bond lengths (Figures 3c and 3d). The calculations, repeated with more water molecules, show no significant change in the vibrational frequencies (Table S4 in the Supporting Information).

Experimental Validation. To validate the theoretical prediction of the formation of iminolate ions, we have performed additional independent experiments. The first experimental evidence of iminolate formation comes from the IR spectrum obtained upon addition of 1 M HCl to the aqueous solution of NMA. O-protonation of amides, stabilized by the resonance structure containing C═N, is well-accepted.

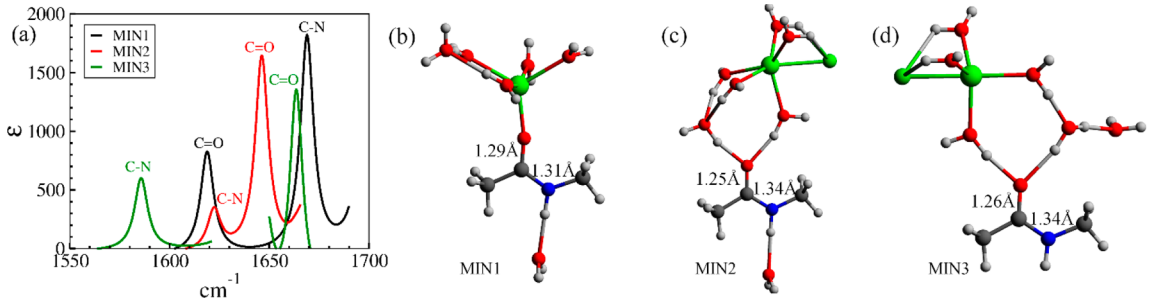

Figure 3. (a) C = O and CN IR frequencies at different Ca^{2+} distances (MIN1 (black), MIN2 (red), and MIN3 (green)). Optimized geometry with the bond length of CO and CN in (b) MIN1, (c) MIN2, and (d) MIN3 conformations, respectively. The molecules (NMA and water) are shown in ball-and-stick model (red = O, white = H, blue = N, green (large) = Ca^{2+}, green (small) = Cl^{-}). The extinction coefficient of CN is greater than that of C═O at MIN3 and less than that of C═O otherwise.

DOI: 10.1021/acs.jpcb.9b08463
J. Phys. Chem. B 2019, 123, 8419−8424

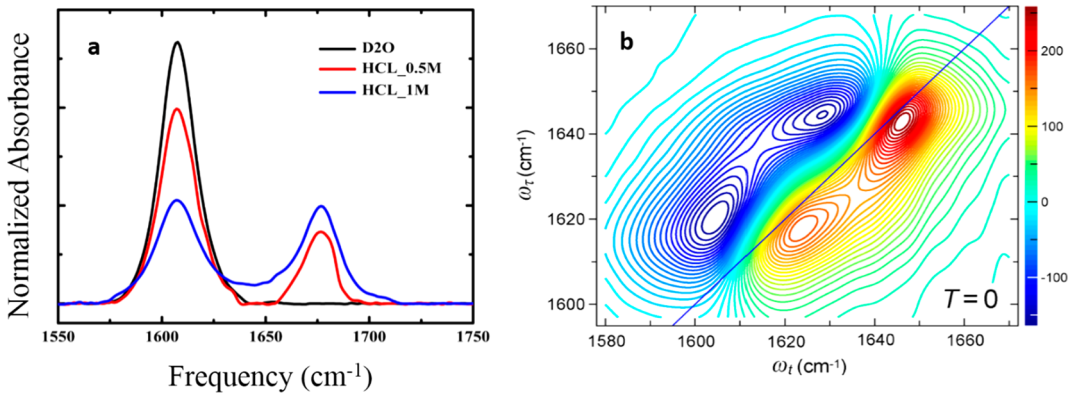

Figure 4. (a) IR spectra of NMA in the presence of acid. The spectrum in neat water (D_2O) is also shown as reference. (b) 2D IR spectrum of an aqueous solution of *N*-methylacetamide in the presence of 5 M $CaCl_2$ at T = 0 (zero waiting time).

We have indeed observed a new blue-shifted population in the presence of the added acid (Figure 4a).

It is well-known that ε is related to the square of the transition dipole strength ($\vec{\mu}$). 2D IR spectroscopy is more sensitive to structural changes than Fourier transform infrared (FTIR) spectroscopy as 2D IR signals are proportional to $|\vec{\mu}^4|$, unlike $|\vec{\mu}^2|$ in FTIR.[34,35] The 2D IR spectrum in Figure 4b consists of two diagonal peak pairs, at 1619 and 1645 cm^{-1}, showing an excellent agreement with the peak positions obtained from the Gaussian profile fits (see Table S1 in the Supporting Information). Moreover, the 2D IR spectrum shows that the blue-shifted peak (1645 cm^{-1}) is more intense than that arising from amide-I (1619 cm^{-1}). This validates the theoretical prediction that the C═N mode has a higher ε value than the C═O stretch. The time evolution of the intensity at the cross peak regions between the two populations in Figure S12 in the Supporting Information probably indicates a population transfer between MIN1 and MIN2. Because of the overlap of the two diagonal peaks and the small diagonal anharmonicity, both time-dependent 2D IR spectra and numerical fitting of the 2D IR spectra will be necessary to comment on the nature and time scale of the population transfer. However, the ultrafast population transfer dynamics is beyond the scope of this work and will be studied separately, supported by statistically significant MD simulations.

CONCLUSION

Numerous studies have implicated Ca^{2+} dysfunction in Alzheimer's disease, demonstrating the bidirectional relationship between Ca^{2+} signaling and the amyloidogenic pathway.[36,37] A recent study has reported that Aβ(1−40) forms oligomers at moderate Ca^{2+} concentrations, as opposed to fibrils in the absence or at low concentrations of Ca^{2+}.[38] However, the mechanism of such a shift in the aggregation pathway in the presence of Ca^{2+} is not known. As backbone hydrogen-bonding (between C═O and NH) is crucial for aggregation,[39] our results indicate Ca^{2+}-bound iminolate tautomers might disrupt the backbone hydrogen bonds to favor the oligomers. However, it is important to note that the Ca^{2+} concentrations used in our studies are substantially higher than the physiological concentration. The variation in the water exposure of the amides in a crowded protein environment (dielectric ∼4) is known to be different from the amide moiety in NMA in aqueous solution (dielectric ∼80). IR experiments of NMA in 1:1 acetonitrile (ACN)/water (dielectric ∼55)[40] apparently shows a 3-fold increase (Figure S13 in the Supporting Information) in the relative population of the contact ion pair when the Ca^{2+} concentration is kept unchanged (2 M). As NMA was immiscible in ACN/water solutions with larger fractions of ACN, the hypothesis could not be tested at a physiological Ca^{2+} concentration. Furthermore, to examine amide/peptide aggregation, we looked into the effect of Ca^{2+} in aggregated NMA (see Figures S14a and S14b in the Supporting Information).[41] Nevertheless, this complete swap of bond orders, arising from amide−iminolate tautomerism, triggered in the presence of divalent cations, is quite unexpected and was never reported in earlier studies. Therefore, the present study throws light into an interesting role of divalent cations in the modulation of the bonding characteristics of the amide group, which might have plausible consequences in biology.

ASSOCIATED CONTENT

Supporting Information

The Supporting Information is available free of charge on the ACS Publications website at DOI: 10.1021/acs.jpcb.9b08463.

Simulation methodology, analysis details (PDF)

AUTHOR INFORMATION

Corresponding Authors

*E-mail: kimys@unist.ac.kr (Y. S. Kim).
*E-mail: arnab.mukherjee@iiserpune.ac.in (A. Mukherjee).
*E-mail: s.bagchi@ncl.res.in (S. Bagchi).

ORCID

Yung Sam Kim: 0000-0001-6306-7438
Arnab Mukherjee: 0000-0001-5691-6120
Sayan Bagchi: 0000-0001-6932-3113

Notes

The authors declare no competing financial interest.

ACKNOWLEDGMENTS

Authors acknowledge SERB India (Nos. EMR/2016/001069 and EMR/2016/000576) and NRF of Korea (No. 2017R1D1A1B03032623) for funding. R.K.M. thanks UGC for fellowship.

REFERENCES

(1) Kunz, W.; Lo Nostro, P.; Ninham, B. W. The Present State of Affairs with Hofmeister Effects. *Curr. Opin. Colloid Interface Sci.* **2004**, *9*, 1−18.

DOI: 10.1021/acs.jpcb.9b08463
J. Phys. Chem. B 2019, 123, 8419−8424

(2) Hofmeister, F. Zur Lehre Von Der Wirkung Der Salze. *Naunyn-Schmiedeberg's Arch. Pharmacol.* **1888**, *24*, 247−260.
(3) Algaer, E. A.; van der Vegt, N. F. A. Hofmeister Ion Interactions with Model Amide Compounds. *J. Phys. Chem. B* **2011**, *115*, 13781−13787.
(4) Zhang, Y.; Furyk, S.; Bergbreiter, D. E.; Cremer, P. S. Specific Ion Effects on the Water Solubility of Macromolecules: PNIPAM and the Hofmeister Series. *J. Am. Chem. Soc.* **2005**, *127*, 14505−14510.
(5) Gurau, M. C.; Lim, S.-M.; Castellana, E. T.; Albertorio, F.; Kataoka, S.; Cremer, P. S. On the Mechanism of the Hofmeister Effect. *J. Am. Chem. Soc.* **2004**, *126*, 10522−10523.
(6) Stirnemann, G.; Wernersson, E.; Jungwirth, P.; Laage, D. Mechanisms of Acceleration and Retardation of Water Dynamics by Ions. *J. Am. Chem. Soc.* **2013**, *135*, 11824−11831.
(7) Funkner, S.; Niehues, G.; Schmidt, D. A.; Heyden, M.; Schwaab, G.; Callahan, K. M.; Tobias, D. J.; Havenith, M. Watching the Low-Frequency Motions in Aqueous Salt Solutions: The Terahertz Vibrational Signatures of Hydrated Ions. *J. Am. Chem. Soc.* **2012**, *134*, 1030−1035.
(8) Omta, A. W.; Kropman, M. F.; Woutersen, S.; Bakker, H. J. Negligible Effect of Ions on the Hydrogen-Bond Structure in Liquid Water. *Science* **2003**, *301*, 347−349.
(9) DeWalt-Kerian, E. L.; Kim, S.; Azam, M. S.; Zeng, H.; Liu, Q.; Gibbs, J. M. pH-Dependent Inversion of Hofmeister Trends in the Water Structure of the Electrical Double Layer. *J. Phys. Chem. Lett.* **2017**, *8*, 2855−2861.
(10) Zhang, Y.; Cremer, P. S. The Inverse and Direct Hofmeister Series for Lysozyme. *Proc. Natl. Acad. Sci. U. S. A.* **2009**, *106*, 15249−15253.
(11) Okur, H. I.; Kherb, J.; Cremer, P. S. Cations Bind Only Weakly to Amides in Aqueous Solutions. *J. Am. Chem. Soc.* **2013**, *135*, 5062−5067.
(12) Shi, J.; Wang, J. Interaction between Metal Cation and Unnatural Peptide Backbone Mediated by Polarized Water Molecules: Study of Infrared Spectroscopy and Computations. *J. Phys. Chem. B* **2014**, *118*, 12336−12347.
(13) Hess, B.; van der Vegt, N. F. A. Cation Specific Binding with Protein Surface Charges. *Proc. Natl. Acad. Sci. U. S. A.* **2009**, *106*, 13296−13300.
(14) Okur, H. I.; Hladílková, J.; Rembert, K. B.; Cho, Y.; Heyda, J.; Dzubiella, J.; Cremer, P. S.; Jungwirth, P. Beyond the Hofmeister Series: Ion-Specific Effects on Proteins and Their Biological Functions. *J. Phys. Chem. B* **2017**, *121*, 1997−2014.
(15) Manak, M. S.; Ferl, R. J. Divalent Cation Effects on Interactions between Multiple Arabidopsis 14−3-3 Isoforms and Phosphopeptide Targets. *Biochemistry* **2007**, *46*, 1055−1063.
(16) Carafoli, E. Calcium Signaling: A Tale for all Seasons. *Proc. Natl. Acad. Sci. U. S. A.* **2002**, *99*, 1115−1122.
(17) Kashid, S. M.; Jin, G. Y.; Bagchi, S.; Kim, Y. S. Cosolvent Effects on Solute-Solvent Hydrogen-Bond Dynamics: Ultrafast 2D IR Investigations. *J. Phys. Chem. B* **2015**, *119*, 15334−15343.
(18) Kashid, S. M.; Jin, G. Y.; Chakrabarty, S.; Kim, Y. S.; Bagchi, S. Two-Dimensional Infrared Spectroscopy Reveals Cosolvent-Composition-Dependent Crossover in Intermolecular Hydrogen Bond Dynamics. *J. Phys. Chem. Lett.* **2017**, *8*, 1604−1609.
(19) Frisch, M. J.; Trucks, G. W.; Schlegel, H. B.; Scuseria, G. E.; Robb, M. A.; Cheeseman, J. R.; Scalmani, G.; Barone, V.; Mennucci, B.; Petersson, G. A., et al. *Gaussian 09*; Gaussian, Inc.: Wallingford, CT, USA, 2009.
(20) Cornell, W. D.; Cieplak, P.; Bayly, C. I.; Kollman, P. A. Application of RESP Charges to Calculate Conformational Energies, Hydrogen Bond Energies, and Free Energies of Solvation. *J. Am. Chem. Soc.* **1993**, *115*, 9620−9631.
(21) Case, D. A.; Cheatham, T. E.; Darden, T.; Gohlke, H.; Luo, R.; Merz, K. M.; Onufriev, A.; Simmerling, C.; Wang, B.; Woods, R. J. The Amber Biomolecular Simulation Programs. *J. Comput. Chem.* **2005**, *26*, 1668−1688.
(22) Sorin, E. J.; Pande, V. S. Exploring the Helix-Coil Transition via All-Atom Equilibrium Ensemble Simulations. *Biophys. J.* **2005**, *88*, 2472−2493.
(23) Yu, H.; Whitfield, T. W.; Harder, E.; Lamoureux, G.; Vorobyov, I.; Anisimov, V. M.; MacKerell, A. D.; Roux, B. Simulating Monovalent and Divalent Ions in Aqueous Solution Using a Drude Polarizable Force Field. *J. Chem. Theory Comput.* **2010**, *6*, 774−786.
(24) Lamoureux, G.; Harder, E.; Vorobyov, I. V.; Roux, B.; MacKerell, A. D., Jr A Polarizable Model of Water for Molecular Dynamics Simulations of Biomolecules. *Chem. Phys. Lett.* **2006**, *418*, 245−249.
(25) Renou, R.; Ding, M.; Zhu, H.; Szymczyk, A.; Malfreyt, P.; Ghoufi, A. Concentration Dependence of the Dielectric Permittivity, Structure, and Dynamics of Aqueous NaCl Solutions: Comparison between the Drude Oscillator and Electronic Continuum Models. *J. Phys. Chem. B* **2014**, *118*, 3931−3940.
(26) Greenwell Yanik, E. Numerical Recipes in FORTRAN—The Art of Scientific Computing 2nd Ed. (W. H. Press, W. T. Vetterling, S. A. Teukolsky and B. P. Flannery). *SIAM Rev.* **1994**, *36*, 149.
(27) Berendsen, H. J. C.; Postma, J. P. M.; van Gunsteren, W. F.; DiNola, A.; Haak, J. R. Molecular Dynamics with Coupling to an External Bath. *J. Chem. Phys.* **1984**, *81*, 3684−3690.
(28) Hess, B.; Bekker, H.; Berendsen, H. J. C.; Fraaije, J. G. E. M. LINCS: A Linear Constraint Solver for Molecular Simulations. *J. Comput. Chem.* **1997**, *18*, 1463−1472.
(29) Darden, T.; York, D.; Pedersen, L. Particle mesh Ewald: An N·log(N) Method for Ewald Sums in Large Systems. *J. Chem. Phys.* **1993**, *98*, 10089−10092.
(30) Hess, B.; Kutzner, C.; van der Spoel, D.; Lindahl, E. GROMACS 4: Algorithms for Highly Efficient, Load-Balanced, and Scalable Molecular Simulation. *J. Chem. Theory Comput.* **2008**, *4*, 435−447.
(31) VandeVondele, J.; Hutter, J. Gaussian Basis Sets for Accurate Calculations on Molecular Systems in Gas and Condensed Phases. *J. Chem. Phys.* **2007**, *127*, 114105.
(32) DeCamp, M. F.; DeFlores, L.; McCracken, J. M.; Tokmakoff, A.; Kwac, K.; Cho, M. Amide I Vibrational Dynamics of N-Methylacetamide in Polar Solvents: The Role of Electrostatic Interactions. *J. Phys. Chem. B* **2005**, *109*, 11016−11026.
(33) Pazos, I. M.; Ghosh, A.; Tucker, M. J.; Gai, F. Ester Carbonyl Vibration as a Sensitive Probe of Protein Local Electric Field. *Angew. Chem., Int. Ed.* **2014**, *53*, 6080−6084.
(34) Dunkelberger, E. B.; Grechko, M.; Zanni, M. T. Transition Dipoles from 1D and 2D Infrared Spectroscopy Help Reveal the Secondary Structures of Proteins: Application to Amyloids. *J. Phys. Chem. B* **2015**, *119*, 14065−14075.
(35) Kim, Y. S.; Hochstrasser, R. M. Chemical Exchange 2D IR of Hydrogen-Bond Making and Breaking. *Proc. Natl. Acad. Sci. U. S. A.* **2005**, *102*, 11185−11190.
(36) Bojarski, L.; Herms, J.; Kuznicki, J. Calcium Dysregulation in Alzheimer's Disease. *Neurochem. Int.* **2008**, *52*, 621−633.
(37) Green, K. N.; LaFerla, F. M. Linking Calcium to Aβ and Alzheimer's Disease. *Neuron* **2008**, *59*, 190−194.
(38) Itkin, A.; Dupres, V.; Dufrene, Y. F.; Bechinger, B.; Ruysschaert, J. M.; Raussens, V. Calcium Ions Promote Formation of Amyloid beta-Peptide (1−40) Oligomers Causally Implicated in Neuronal Toxicity of Alzheimer's Disease. *PLoS One* **2011**, *6*, No. e18250.
(39) Nelson, R.; Sawaya, M. R.; Balbirnie, M.; Madsen, A. Ø.; Riekel, C.; Grothe, R.; Eisenberg, D. Structure of the Cross-B Spine of Amyloid-Like Fibrils. *Nature* **2005**, *435*, 773−778.
(40) Langhals, H. Polarity of Binary Liquid Mixtures. *Angew. Chem., Int. Ed. Engl.* **1982**, *21*, 724−733.
(41) Cunha, A. V.; Salamatova, E.; Bloem, R.; Roeters, S. J.; Woutersen, S.; Pshenichnikov, M. S.; Jansen, T. L. C. Interplay between Hydrogen Bonding and Vibrational Coupling in Liquid N-Methylacetamide. *J. Phys. Chem. Lett.* **2017**, *8*, 2438−2444.

DOI: 10.1021/acs.jpcb.9b08463
J. Phys. Chem. B 2019, 123, 8419−8424